J|A|C|S
ARTICLES
Published on Web 11/16/2002

Photophysical Properties of Porphyrin Tapes

Hyun Sun Cho,[†] Dae Hong Jeong,[†] Sung Cho,[†] Dongho Kim,*[,†] Yoichi Matsuzaki,[‡] Kazuyoshi Tanaka,[§] Akihiko Tsuda,[||] and Atsuhiro Osuka*[,||]

Contribution from the Center for Ultrafast Optical Characteristics Control and Department of Chemistry, Yonsei University, Seoul 120-749, Korea, Advanced Technology Research Laboratories, Nippon Steel Corporation, 20-1 Shintomi, Futtsu, Chiba 293-8511, Japan, Department of Molecular Engineering, Graduate School of Engineering, Kyoto University, Sakyo-ku, Kyoto 606-8501, Japan, and Department of Chemistry, Kyoto University, Kyoto 606-8502, Japan

Received June 10, 2002. Revised Manuscript Received August 29, 2002

Abstract: The novel fused Zn(II)porphyrin arrays (**Tn**, porphyrin tapes) in which the porphyrin macrocycles are triply linked at *meso*−*meso*, $\beta-\beta$, $\beta-\beta$ positions have been investigated by steady-state and time-resolved spectroscopic measurements along with theoretical MO calculations. The absorption spectra of the porphyrin tapes show a systematic downshift to the IR region as the number of porphyrin pigments increases in the arrays. The fused porphyrin arrays exhibit a rapid formation of the lowest excited states (for **T2**, ∼500 fs) via fast internal conversion processes upon photoexcitation at 400 nm (Soret bands), which is much faster than the internal conversion process of ∼1.2 ps observed for a monomeric Zn(II)-porphyrin. The relaxation dynamics of the lowest excited states of the porphyrin tapes were accelerated from ∼4.5 ps for the **T2** dimer to ∼0.3 ps for the **T6** hexamer as the number of porphyrin units increases, being explained well by the energy gap law. The overall photophysical properties of the porphyrin tapes were observed to be in a sharp contrast to those of the orthogonal porphyrin arrays. The PPP−SCI calculated charge-transfer probability indicates that the lowest excited state of the porphyrin tapes (**Tn**) resembles a Wannier-type exciton closely, whereas the lowest excited state of the directly linked porphyrin arrays can be considered as a Frenkel-type exciton. Conclusively, these unique photophysical properties of the porphyrin tapes have aroused much interest in the fundamental photophysics of large flat organic molecules as well as in the possible applications as electric wires, IR sensors, and nonlinear optical materials.

I. Introduction

Porphyrin-based molecules have been extensively studied over recent years, primarily due to their importance in biological systems.[1] Moreover, their versatile optical and electrochemical properties, the possibility to tune these properties by incorporating different metals into the center of the ring or by grafting various substituents at their peripheral positions, and their high chemical and thermal stabilities make porphyrins attractive materials in electronics, optoelectronics, and photonics.[2] In these respects, conjugated porphyrin arrays have been demonstrated more promising owing to their attributes such as red-shifted absorption bands, large nonlinear optical properties, and exceptionally large π-electron delocalization.[3] Two types of conjugated porphyrin arrays including ethyne-[4] or butadiyne-bridged[5] porphyrin arrays and fused porphyrin arrays[6−11] have been developed, exhibiting favorable properties for the above purposes.

In the course of our research projects of exploring novel pophyrin arrays, we have prepared directly *meso*−*meso* linked

* To whom all the correspondence should be addressed. E-mails: dongho@yonsei.ac.kr; osuka@kuchem.kyoto-u.ac.jp.

[†] Center for Ultrafast Optical Characteristics Control and Department of Chemistry, Yonsei University.

[‡] Advanced Technology Research Laboratories, Nippon Steel Corporation.

[§] Department of Molecular Engineering, Graduate School of Engineering, Kyoto University.

[||] Department of Chemistry, Kyoto University.

(1) (a) Wasielewski, M. R. *Chem. Rev.* **1992**, *92*, 435. (b) Osuka, A.; Mataga, N.; Okada, T. *Pure Appl. Chem.* **1997**, *69*, 797.

(2) Chou, J.-H.; Nalwa, H. S.; Kosal, M. E.; Rakow, N. A.; Suslick, K. S. In *The Porphyrin Handbook*; Kadish, K. M., Smith, K. M., Guilard, R., Eds; Academic Press: San Diego, 2000; Vol. 6, Chapter 41.

(3) (a) Arnold, D. P.; Johnson, A. W.; Mahendran, M. *J. Chem. Soc., Perkin Trans. 1* **1978**, 366. (b) Anderson, H. L. *Inorg. Chem.* **1994**, *33*, 972. (c) Lin, V. S.-Y.; DiMagno, S. G.; Therien, M. J. *Science* **1994**, *264*, 1105. (d) Arnold, D. P.; Heath, G. A.; James, D. A. *J. Por. Phthal.* **1999**, *3*, 5. (e) Wilson, G. S.; Anderson, H. L. *Chem. Commun.* **1999**, 1539.

(4) (a) Graça, M.; Vicente, H.; Jaquinod, L.; Smith, K. M. *Chem. Commun.* **1999**, 1771. (b) Anderson, H. L. *Chem. Commun.* **1999**, 2323, and references therein.

(5) (a) Taylor, P. N.; Wylie, A. P.; Huuskonen, W. J.; Anderson, H. L. *Angew. Chem., Int. Ed. Engl.* **1998**, *37*, 986. (b) Blake, I. M.; Rees, L. H.; Claridge, T. D. W.; Anderson, H. L. *Angew. Chem., Int. Ed.* **2000**, *39*, 1818.

(6) (a) Crossley, M. J.; Burn, P. L. *J. Chem. Soc., Chem. Commun.* **1987**, 39. (b) Reimers, J. R.; Lü, T. X.; Crossley, M. J.; Hush, N. S. *Chem. Phys. Lett.* **1996**, *256*, 353.

(7) Kobayashi, N.; Numao, M.; Kondo, R.; Nakajima, S.; Osa, T. *Inorg. Chem.* **1991**, *30*, 2241.

(8) Paolesse, R.; Jaquinod, L.; Della, S.; Nurco, D. J.; Prodi, L.; Montalti, M.; Natale, C. D.; D′Amico, A.; Carlo, A. D.; Lugli, P.; Smith, K. M. *J. Am. Chem. Soc.* **2000**, *122*, 11 295.

(9) Richeter, S.; Jeandon, C.; Ruppert, R.; Callot, H. J. *Chem. Commun.* **2001**, 91.

(10) (a) Tsuda, A.; Nakano, A.; Furuta, H.; Yamochi, H.; Osuka, A. *Angew. Chem., Int. Ed.* **2000**, *39*, 558. (b) Tsuda, A.; Furuta, H.; Osuka, A. *Angew. Chem., Int. Ed.* **2000**, *39*, 2549. (c) Tsuda, A.; Furuta, H.; Osuka, A. *J. Am. Chem. Soc.* **2001**, *123*, 10 304.

(11) Tsuda, A.; Osuka, A. *Science* **2001**, *293*, 79.

10.1021/ja020826w CCC: $22.00

Chart 1

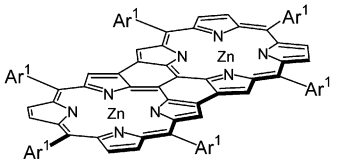

1

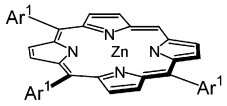

2

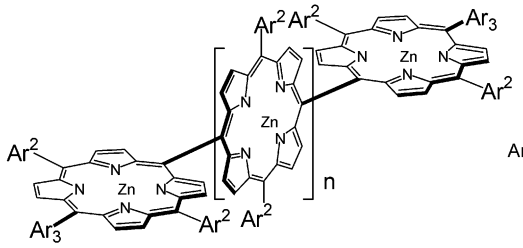

S2 n=0
S3 n=1
S4 n=2
S5 n=3
S6 n=4
S8 n=6
S12 n=10

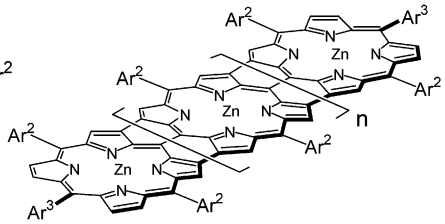

T2 n=0
T3 n=1
T4 n=2
T5 n=3
T6 n=4
T8 n=6
T12 n=10

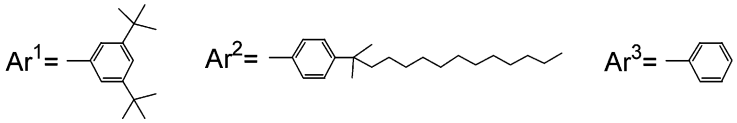

Zn(II)porphyrin arrays **Sn** (Chart 1) up to 128-mer, whose photophysical properties have been revealed, through various measurements, to depend on the length of the arrays and to be characterized by the radiative coherent length of ca. 6−8.[12,13] These linear porphyrin arrays maintain an orthogonal conformation between the neighboring porphyrin units with small conformational heterogeneity.[13] Overall, these arrays can be a promising photonic wire by transmitting singlet excitation energy rapidly over the array mediated by ample electronic interactions between the neighboring porphyrin moieties. These arrays, however, are expected to exhibit poor electrical conductivity due to the relatively high HOMO−LUMO band gap energy because the orthogonal conformation disrupts π-electron conjugation.

In a next step, we employed a combination of DDQ (2,3-dichloro-5,6-dicyano-1,4-benzoquinone) and $Sc(OTf)_3$ (scandium trifluoromethanesulfonate) as an effective oxidant that enabled the smooth transformation of *meso*-phenyl capped *meso*−*meso*-linked porphyrin arrays into *meso*−*meso*, β-β, β-β triply linked porphyrin arrays (**Tn**, porphyrin tapes, Chart 1). The porphyrin tapes thus prepared are indeed exceptional molecules because the lowest absorption band becomes increasingly red-shifted with an increase of the number of the porphyrin moieties without indication of the effective conjugation length (ECL) at least up to **T12**. As an extreme case, **T12** exhibits very low optical HOMO−LUMO gap of ca. 1500 cm^{-1}. These properties are in contrast with the previously reported conjugated porphyrin arrays, which show a conjugation saturation behavior due to ECL and exhibit the optical HOMO−LUMO gaps of ca. 12 000 cm^{-1} at least. Here, it is worthwhile to note that most of organic π-conjugated systems encounter ECL effect, except only limited cases such as cyanine and oxanol dyes[14] and [*n*]acenes[15] (n = 1 to 7), both of which have proven to overcome the ECL effect by escaping from bond alternation within a confined pigment number. With these in background, the photophysical properties of the porphyrin tapes are intriguing not only in view of their potential applications as nonlinear optical materials, infrared (IR) dyes, optical limiters, and optoelectronic devices, but also in view of basic curiosity how such extremely conjugated π-electronic systems behave in their excited states.

The prospect of performing all optical switching via the intensity-dependent refractive index change is particularly attractive for optical communications and data-processing applications.[16] However, suitable material has yet to be convincingly demonstrated as having a full range of required attributes.

(12) (a) Aratani, N.; Osuka, A.; Kim, D.; Kim, Y. H.; Jeong, D. H. *Angew. Chem.* **2000**, *39*, 1458. (b) Kim, Y. H.; Jeong, D. H.; Kim, D.; Jeoung, S. C.; Cho, H. S.; Kim, S. K.; Aratani, N.; Osuka, A. *J. Am. Chem. Soc.* **2001**, *123*, 76. (c) Kim, Y. H.; Cho, H. S.; Kim, D.; Kim, S. K.; Yoshida, N.; Osuka, A. *Synth. Metal* **2001**, *117*, 183. (d) Aratani, N.; Osuka, A.; Cho, H. S.; Kim, D. *J. Photochem. Photobiol. C: Photochem. Rev.* **2002**, *3*, 25.

(13) Cho, H. S.; Song, N. W.; Kim, Y. H.; Jeoung, S. C.; Hahn, S.; Kim, D.; Kim, S. K.; Yoshida, N.; Osuka, A. *J. Phys. Chem. A* **2000**, *104*, 3287.

(14) Kuhn, H. *J. Chem. Phys.* **1949**, *17*, 1198.

(15) (a) Martin, R. E.; Diederich, F. *Angew. Chem., Int. Ed. Engl.* **1999**, *38*, 1351. (b)Clar, E. *Ber. Dtsch, Chem. Ges.* **1936**, *69*, 607.

Preliminary electroabsorption studies and simple MO calculations of **Tn** have suggested their high potentials as nonlinear optical material. The response time of the optical nonlinearity is also crucial for ultrafast switching systems and is desirably short compared with the period of an optical switching cycle. Here, on the basis of the ultrafast time-resolved spectroscopic measurements, we examined the excited-state properties of the porphyrin tapes that are extremely short-lived, being favorable for the above purpose.

II. Experimental Methods

Synthesis of Fused Porphyrin Arrays. The details of the synthetic and purification procedures of the fused porphyrin arrays were given elsewhere.[10,11] Basically, the oxidative double-ring closure (ODRC) reaction of *meso*−*meso*-linked Zn(II)-porphyrin arrays yields the corresponding porphyrin tapes, **Tn**. The ODRC reaction was conducted by refluxing a solution of *meso*,*meso*-diphenyl-capped *meso*−*meso* linked porphyrin array in toluene in the presence of 2,3-dichloro-5,6-dicyano-1,4-benzoquinone and scandium trifluoromethanesulfonate. This type of ODRC reaction was nicely applied to longer fused porphyrin arrays. For reference porphyrin arrays, we used *meso*−*meso* linked porphyrin arrays, **Sn** (Chart 1).

Transient Absorption Experimental Setup. The dual-beam femtosecond time-resolved transient absorption spectrometer consisted of a self-mode-locked femtosecond Ti:sapphire oscillator (Coherent, MIRA), a Ti:sapphire regenerative amplifier (Clark MXR, CPA-1000) pumped by a Q-switched Nd:YAG laser (Clark MXR, ORC-1000), a pulse stretcher/compressor, OPA (Light Conversion, TOPAS) system, and an optical detection system. A femtosecond Ti:sapphire oscillator pumped by a CW Nd:YVO_4 laser (Coherent, Verdi) produces a train of ∼80 fs mode-locked pulses with an averaged power of 650 mW at 800 nm. The amplified output beam regenerated by chirped pulse amplification (CPA) had ca. 150 fs pulse width and a power of ca. 1 W at 1 kHz repetition rate, which was divided into two parts by a 1:1 beam splitter. One was color-tuned for the pump beam by optical parametric generation and amplification (OPG−OPA) technique. The resulting laser pulse had a temporal width of ∼150 fs in the UV/vis/IR range. The pump beam was focused to a 1 mm diameter spot and the laser fluence was adjusted to avoid the damage of sample by using a variable neutral-density filter. The other was focused onto a flowing water cell to generate a white light continuum, which was again split into two parts. The one part of the white-light continuum was overlapped with the pump beam at the sample to probe the transient, whereas the other part of the beam was passed through the sample without overlapping the pump beam. The time delay between pump and probe beams was controlled by making pump beam travel along a variable optical delay. The white light continuum beams after the sample were sent to a 15 cm focal length spectrograph (Acton Research) through each optical fiber and then detected by a dual-channel 512 channel photodiode array (Princeton Instruments). The intensity of the white light continuum of each 512 channel photodiode array was processed to calculate the absorption difference spectrum at the desired time delay between pump and probe pulses.

Femtosecond Fluorescence Upconversion Setup. The amplified output is divided by a 1:1 beam splitter into two parts. One of them was frequency-doubled by a 0.5 mm LBO crystal to produce the excitation pulses at 400 nm. The excitation beam was loosely focused onto the sample with a spot size of ∼1 mm by a concave mirror. The luminescence was collected and focused onto a 1 mm BBO crystal by two identical parabolic mirrors ($f = 70$ mm, $d = 50$ mm). The other part of fundamental laser beam was focused onto the BBO crystal with a spatial overlap with the focused emission spot. The time-delay between pump and gate pulses was controlled with a computer-driven optical delay line. The up-converted UV light was focused onto the entrance slit of a monochromator (Jovin−Yvon, HR320). The scattered light was filtered out with a combination of pinhole and appropriate color filters. The instrumental response was estimated to be ∼250 fs from the cross-correlation function between pump and gate beams.

The output current from a photomultiplier tube (Hamamatsu) was amplified with a fast preamplifier, and then the output voltage was fed into a Boxcar averager (SR250). The resultant signal modulated by a chopper was phase-sensitively measured by a lock-in-amplifier (EG&G) and then fed into a personal computer for further data processing. Much care was taken to avoid a possible saturation of photomultiplier tube due to the short duration of up-converted UV light even though its average power is very low.

Molecular Orbital Calculation. To understand the photophysical properties of the fused porphyrin arrays, we calculated the electronic excited states of unsubstituted fused porphyrin arrays by the single-configuration interaction (SCI) method on the basis of the Pariser−Parr−Pople (PPP) Hamiltonian.[17,18] The molecular geometry of **Tn** was constructed as follows: the geometry of each porphyrin subunit was fixed to that derived from the X-ray data of Zn(II)tetraphenylporphyrin[19] and these subunits were arranged keeping the *meso*-*meso* bond length of 1.51 Å as found in the X-ray structure of fused Zn(II)porphyrin dimer,[10(b)] which leads to the $\beta-\beta$ distance of 1.455 Å being close to the value of 1.44 Å in the X-ray structure. The PPP parameters for carbon and nitrogen were taken from the "traditional" set in ref 20 (Zn is not explicitly included since it has no valence π electron). The first-neighbor transfer integrals were evaluated on the basis of the assumed geometry[20] except that for the $\beta-\beta$ linkage in **Tn** which is based on the experimental bond length (1.44 Å). The inter-site Coulomb interactions were evaluated by the Nishimoto−Mataga formula.[21] Note that all the one-electron levels are considered in the SCI expansion taking advantage of the molecular D_{2h} symmetry to reduce the dimension of the Hamiltonian matrix which should be diagonalized. We assume that the molecule is located on the *xy* plane with the long molecular axis set to the *x* axis.

Within the SCI scheme, the atomic-orbital (AO) representation, which is equivalent to the site representation under the PPP approximation, of the transition density matrix corresponding to an excited state *e* is given by

(16) Stegeman, G.; Likamwa, P. In *Nonlinear Optical Materials and Devices for Applications in Information technology*; Miller, A., Welford, K. R., Daino, B., Eds.; Kluwer Acad. Publ.; Dordrecht, 1995; Vol. 289, pp 285−320.

(17) Pariser, R.; Parr, R. G. *J. Chem. Phys.* **1953**, *21*, 767.
(18) Pople, J. A. *Trans. Faraday Soc.* **1953**, *42*, 1375.
(19) Sekino, H.; Kobayashi, H. *J. Chem. Phys.* **1987**, *86*, 5045.
(20) Weiss, C.; Kobayashi, H.; Gouterman, M. *J. Mol. Spectrosc.* **1965**, *16*, 415.
(21) Nishimoto, K.; Mataga, N. *Z. Phys. Chem.* **1957**, *12*, 335.

$$\rho_{rs} = \sqrt{2}\sum_i \sum_a Y_i^a(e) C_{ri} C_{sa} \quad (1)$$

where $Y_i^a(e)$ is the SCI expansion coefficient associated with *i* (occupied MO) to *a* (unoccupied MO) transition and C_{ri} is the LCAO (linear combination of AO) coefficient in *i*-th MO. To characterize each excited state in terms of charge-transfer (CT) nature, we calculate the charge-transfer probability $\boldsymbol{P}_{e-h}$ defined by

$$P_{e-h}(r, s) = {\rho_{rs}}^2/2 \quad (2)$$

which represents the probability of simultaneously finding an electron at *r* and a hole at *s*.[22] Note that the orthonormalization of AOs assumed in the present scheme ensures $\sum_{r,s} P_{e-h}(r,s) = 1$. For comparison, such analysis is also performed on the electronic excited states of **S8** which is composed of mutually orthogonal porphyrin subunits; therefore, the transfer integral is vanished at the *meso*−*meso* linkage. Although they provide no significant effect on the linear absorption spectrum of **S8**, we include intersubunit transfer integrals at the α−α, α−*β*, and *β*−*β* carbon pairs (their magnitudes are ca. 0.05 eV).

III. Results

Steady-State Absorption Spectra of Fused Porphyrin Arrays. Figure 1 shows the UV/vis/IR absorption spectra of **Sn** and **Tn** in $CHCl_3$ normalized at 23 700 to 24 000 cm^{-1} and 23 800 to 24 600 cm^{-1} regions, respectively. As reported in our previous works,[12,13] the Soret bands of **Sn** exhibit splitting due to the exciton coupling between the adjacent porphyrin units with a large coupling energy of approximately 4300 cm^{-1} (Figure 1a). But their Q-bands remain nearly at the same positions. These spectral features have been ascribed mainly to the perpendicular conformation that disrupts *π*-electron conjugation between the adjacent porphyrins.[13] On the contrary, the conjugated porphyrin tapes **Tn** display drastically red-shifted absorption spectra that reach into infrared region. The absorption bands of **Tn** are roughly categorized into three distinct well-separated subgroups, which are marked as bands I, II, and III, respectively, in near UV, visible, and IR regions just for convenience (Figure 1b). With an increase in the number of the porphyrin moieties, the bands I remain nearly the same positions as that of Zn(II)porphyrin monomer with significant broadening, whereas the bands II and III are continuously red-shifted along with an increase in their band intensities (Figure 1b). The peak positions for the bands II as a function of the number of porphyrin moieties indicate that the bands II exhibit a clear saturation behavior with the ECL number of ca. 8, whereas the bands III do not exhibit such a saturation behavior and the ECL number cannot be defined at least up to **T12**.

MO Calculation of Electronic Excited States of Fused Porphyrin Arrays. Figure 2 shows the frontier eight orbitals (the highest four occupied and the lowest four unoccupied) for **T2** together with their energy levels as obtained by the PPP self-consistent field (SCF) calculation. As can be seen, these eight orbitals are formed by the combinations of monomer's four frontier orbitals[23] and their energy levels significantly split relative to their bonding and antibonding *π*−*π* interactions at the two *β*−*β* linkages and especially at the *meso*−*meso* linkage. For comparison, also plotted in Figure 2 are the MO levels of **T2(*m*−*m*)** which has the same geometry as that of **T2** except no *π*-conjugation at the two *β*−*β* linkages. Although **T2(*m*−*m*)** is a hypothetical molecule, its electronic structure would roughly represent that of *meso*−*meso* butadiyne-linked porphyrin dimer.[5] It is evident that the additional *β*−*β* *π*-conjugation leads to further stabilization of the LUMO relative to the case of only *meso*−*meso* conjugation implying that the *meso*−*meso*, *β*−*β*, *β*−*β* triply linked porphyrin dimer is quite promising as a building block element for small HOMO−LUMO energy-gap material. The transition properties of low-lying excited states of **T2** are summarized in Table 1. Based on the present calculation, the III, II, and I absorption bands are assigned to the $1B_{3u}$, $2B_{3u}$, and $4B_{2u}$ states. In the theoretical studies of **S2**,[24] we found that eight charge-transfer (CT) excited states are accidentally located in the energy region spanned by the split Soret bands. These CT states are described as one-electron transition from the a_{1u} or a_{2u} MO of one unit to one of the e_g MOs of the other unit. Because the energy level of the CT state should strongly depend on the intersubunit distance, the quasi-degeneracy of the CT and Soret bands is quite specific to the direct linkage of the porphyrin subunits. As shown in Table 1, those states labeled by "CT" are clearly characterized to be such CT states on the basis of their P_{CT} and W_8 values. Because the extended *π*-conjugation of **T2** generally causes a significant mixing of localized exciton (LE) and CT nature and a contribution of transitions beyond the eight-orbital space becomes rather significant even for low-lying excited states, a complete assignment of all of the eight CT states is difficult for **T2** in contrast to the case of **S2**.

The energy levels of all the excited states including dipole-forbidden states are shown in Figure 3. It is noteworthy that the number of excited states in the energy region between the bands I and II is apparently larger than 2*N* (*N* stands for the number of porphyrin subunits) which is expected from the two Soret components in each subunit. The absorption spectra of the porphyrin tapes are qualitatively reproduced by the calculation. On the basis of the SCI expansion of the states I, II, and III for **T2**, it is regarded that the bands I and II arise from the Soret band of a monomer while the band III originates from the monomer's Q-band. The calculation indicates that the transition dipole moment is parallel to the long molecular *x* axis for the bands II and III, whereas it is aligned along the short molecular *y* axis for the band I. Then, the splitting of the Soret band into the bands I and II is qualitatively consistent with the exciton-coupling scheme. In addition, the overestimation of the energies of the bands I and II can be attributed to a situation that the present method overestimates the Soret band energy of a porphyrin monomer by 0.5 eV relative to the experimental value. One possible reason for this discrepancy would be the lack of *σ*−*π* interaction in the present computational scheme.

The band III corresponds to an excitation to the lowest excited singlet state. The significant intensification of the bands III relative to the bands I and II in **Tn** is in contrast to the case of monomer where the *Q*(0,0) absorption is very weak due to the

(22) (a) Mukamel, S.; Tretiak, S.; Wagersreiter, T.; Chernyak, V. *Science* **1997**, *277*, 781. (b) Zojer, E.; Buchacher, P.; Wudl, F.; Cornil, J.; Calbert, J. Ph.; Brédas, J. L.; Leising, G. *J. Chem. Phys.* **2000**, *113*, 10 002.
(23) Gouterman, M. *J. Chem. Phys.* **1959**, *30*, 1139.
(24) (a) Yoshida, N.; Jeong, D. H.; Cho, H. S.; Kim, D.; Matsuzaki, Y.; Tanaka, K.; Osuka, A. *Chem. Eur. J.* In press. (b) Jeong, D. H.; Jang, S. M.; Hwang, I.-W.; Kim, D.; Yoshida, N.; Osuka, A. *J. Phys. Chem.* In press.

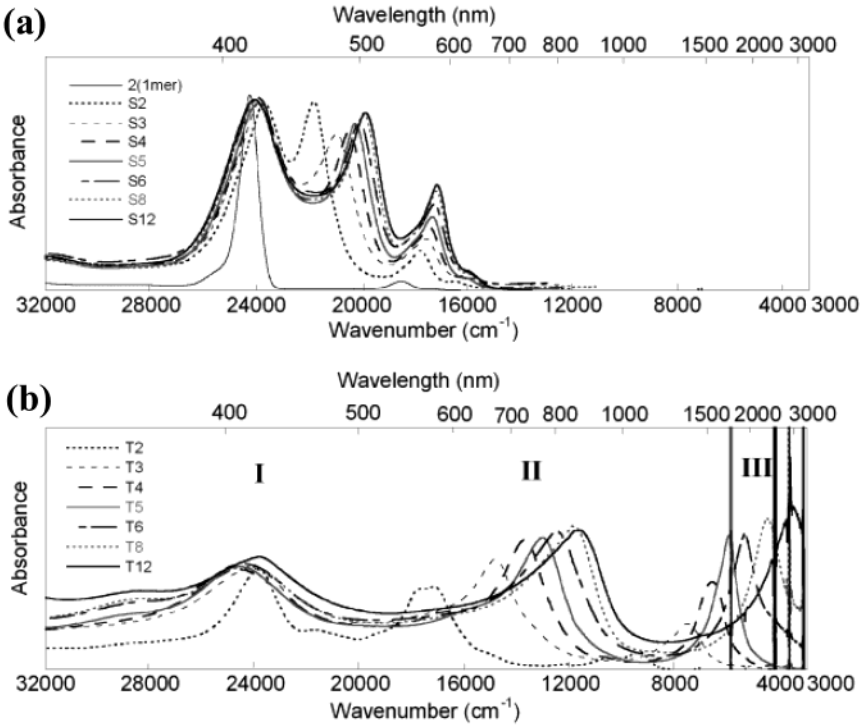

Figure 1. Ultraviolet-visible-infrared absorption spectra of porphyrin monomer **2** and *meso*−*meso*-linked porphyrin arrays from **S2** to **S12** (top) and triply linked fused porphyrin arrays from **T2** to **T12** (bottom) taken in $CHCl_3$ at room temperature. The background absorption at ∼6000, ∼4000, ∼3500 cm^{-1} may arise from the overtones of C−H vibration of the solvent.

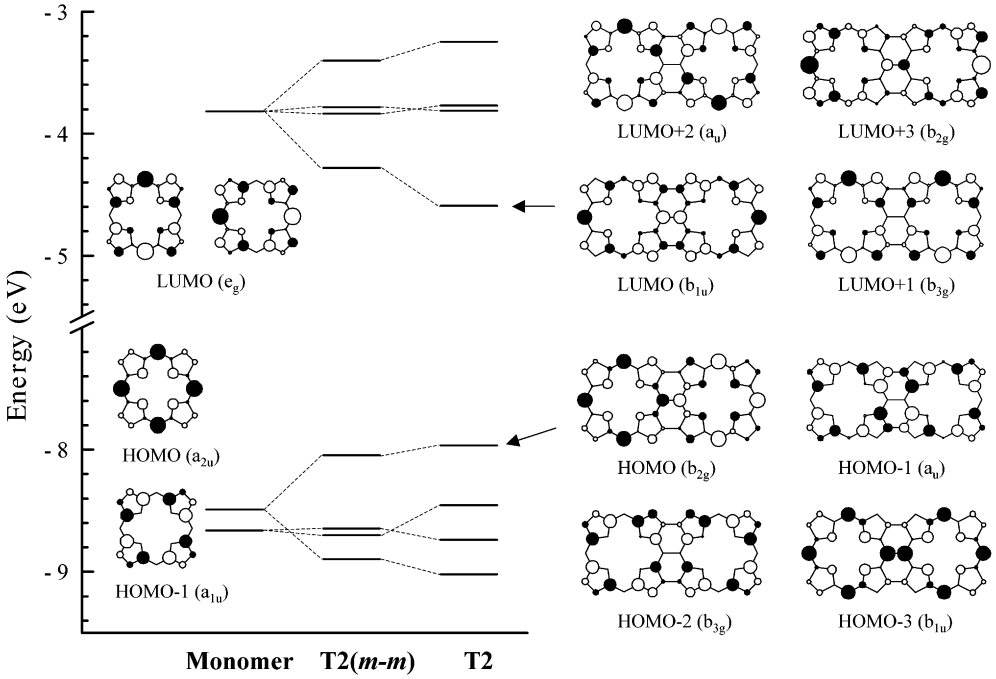

Figure 2. Frontier eight orbitals and their energy levels for **T2**, which were obtained by the PPP self-consistent field (SCF) calculation. For comparison, the MO levels were shown for **T2(m−m)**, which has the same geometry as that of **T2** except no π-conjugation at $\beta-\beta$ linkages.

accidental cancellation of the transition dipole moments of $^1(a_{1u},e_g)$ and $^1(a_{2u},e_g)$ configurations. In **Tn**, the efficient π-conjugation along the *x*-axis lifts the accidental cancellation of the transition dipole moments of the bands III, hence intensifying the absorption bands. The SCI expansion coefficients for the main excited states of **T2** are listed in Table 2. We note that for the $1B_{3u}$ state (band III), the contribution of HOMO → LUMO transition overwhelms that of HOMO − 1 → LUMO + 1 transition and the former carries much larger transition dipole moment than the latter. This situation should be caused by efficient π-electron delocalization along the long molecular axis (*x*) being responsible for the intensification of the band III for **T2**. In contrast, the above-mentioned Q-band nature is well retained for the $1B_{2u}$ state which also arises from the monomer's Q-band but is polarized in the *y* direction. For both $2B_{3u}$ and $4B_{2u}$ states, the component transition dipole

Table 1. Transition Properties and Electronic Structures of the Lowest 18 Singlet excited states of **T2**, as obtained from PPP−SCI Calculations

band	state	ΔE (eV)[a]	f[b]	P_{CT} (%)[c]	W_8 (%)[d]	comments[e]
III	$1B_{3u}$	1.41 (1.16)	0.517 (*x*)	33	96	Q
	$1B_{1g}$	1.52	0	34	97	Q
	$1B_{2u}$	1.77	0.002 (*y*)	21	97	Q
	$2A_g$	1.98	0	12	96	Q
	$2B_{1g}$	2.24	0	33	81	
II	$2B_{3u}$	2.65 (2.13)	3.922 (*x*)	23	93	Soret
	$3A_g$	2.72	0	68	93	CT
	$2B_{2u}$	2.79	0.694 (*y*)	68	93	CT
	$3B_{3u}$	2.88	0.382 (*x*)	46	19	
	$3B_{1g}$	3.04	0	59	52	
	$4A_g$	3.15	0	81	90	CT
	$3B_{2u}$	3.21	0.153 (*y*)	67	92	CT
	$4B_{3u}$	3.22	0.215 (*x*)	76	75	CT
	$4B_{1g}$	3.38	0	57	52	
	$5B_{3u}$	3.61	1.032 (*x*)	21	22	
I	$4B_{2u}$	3.64 (2.97)	3.415 (*y*)	9	73	Soret
	$5B_{1g}$	3.68	0	13	69	Soret
	$5A_g$	3.68	0	11	83	Soret

[a] Excitation energy. The experimental values are listed in parentheses. [b] Oscillator strength. The direction of transition dipole moment is indicated in parentheses. [c] Inter-unit charge-transfer probability defined by $P_{CT} = \sum_{I\neq J}\sum_{r\in I}\sum_{s\in J}P_{e-h}(r,s)$ where $I(J)$ represents one porphyrin subunit in a dimer. [d] The weight of the transitions within eight-orbitals in the SCI wave function. [e] The excited states arising from monomer's Q and Soret states are labeled by "Q" and "Soret", respectively. For the explanation of "CT", see text.

moments are coupled to enhance each other as in the case of the monomer's Soret band.

In addition, the calculation shows that the band II comprises of several dominant transitions and the band I consists of many absorption bands especially for longer arrays. These computational results are consistent with more significant broadening observed for the bands I and II (especially the former) as compared with the bands III (compare Figure 1 with Figure 3). These spectral features illustrate efficient π-electron delocalization in the porphyrin tapes, since a simple dipole−dipole interaction between the Soret transitions on the adjacent chromophores should lead to much sharp bandwidth.

In the case of **T2**, we have confirmed that six CT states are located in the energy region between the I and II states on the basis of their charge-transfer probability $\boldsymbol{P}_{e-h}$ which is defined by eqs 1 and 2. For longer arrays, these CT states as well as the Soret states establish a band of intermediate levels closely located to each other as seen in Figure 3 and Table 1. We note that the main contribution to the enhanced absorption in the interval region between the bands I and II arises from the moderate oscillator strength of the CT band, which is a result of significant configuration mixing of localized exciton (LE) character into the CT states caused by efficient π-conjugation in the fused porphyrin arrays. In addition, it is worthwhile to point out that the absorption band on the high-energy side of the band I is also reproduced by the present PPP−SCI calculation.

Excited-State Dynamics of Fused Porphyrin Dimer. Because the light energy transfer process in molecular wires occurs through the excited-state energy transfer, it is relevant to gain further insight into how the energy hopping process occurs in the excited states of the molecular wires. As **Tn** exhibits a systematic change in the absorption spectra with three distinct absorption bands, femtosecond UV/vis/IR pump/probe experiments upon selective photoexcitation of each band were carried out to investigate the electronic energy relaxation process of

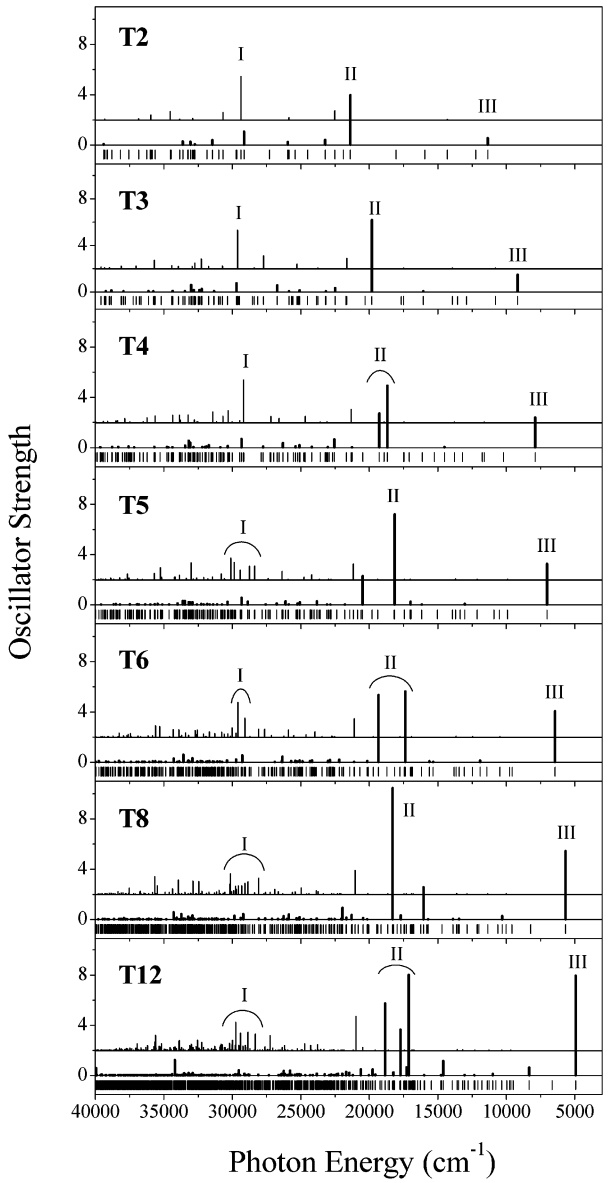

Figure 3. PPP−SCI simulated electronic absorption spectra for the fused porphyrin arrays. The optical transitions along the *x* and *y* axes are indicated in thick and thin solid lines, respectively. The optical transitions along the *y* axis are offset vertically by an oscillator strength value of 2.0 for a clear presentation. The molecule is in the *xy* plane with the long molecular axis set to the *x* axis. The energy levels of all the excited states are marked in the negative oscillator strength region for each array.

Table 2. PPP−SCI Expansion Coefficients in the Description of the Singlet Excited States of T2[a]

transition		$1B_{3u}$	$1B_{2u}$	$2B_{3u}$	$4B_{2u}$
H → L	19.08[a]	0.87		0.42	
H-1 → L+1	12.17	−0.34		0.72	
H-2 → L+2	10.74	−0.24		0.44	
H-3 → L+3	4.32	0.16		−0.18	
H → L+2	−11.90		0.63		0.25
H-2 → L	12.11		0.67		−0.30
H-1 → L+3	10.01		0.24		−0.53
H-3 → L+1	−8.66		0.28		0.54

[a] H denotes the HOMO level and L the LUMO. [b] Transition dipole moment (in Debye) of each configuration function.

each state (band I (near UV), band II (visible/near-IR), and band III (near-IR/IR)). Figure 4 shows the transient absorption spectra of **T2**∼**T6** upon photoexcitation at 400 nm which is in resonance

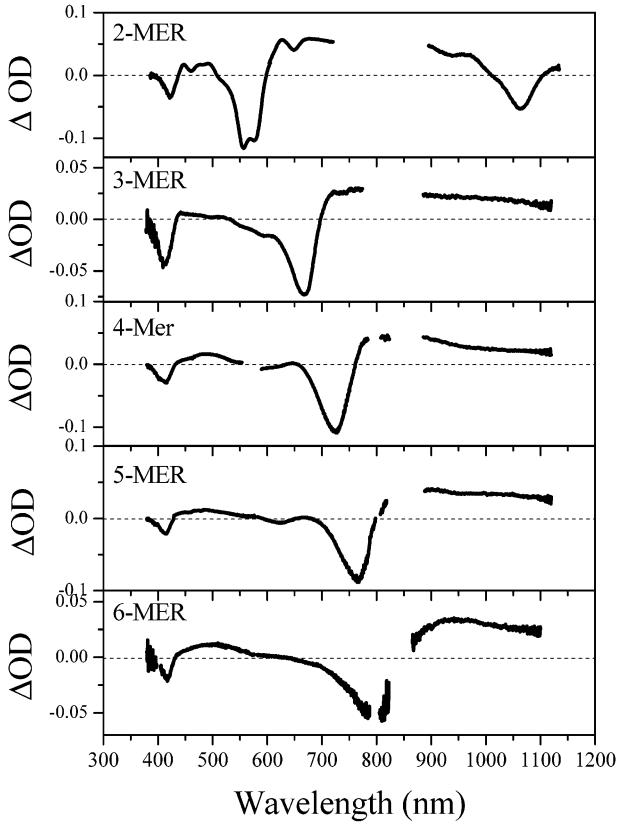

Figure 4. Transient absorption spectra of **T2**, **T3**, **T4**, **T5**, and **T6** from top to bottom at zero delay time between pump and probe pulses in toluene. The ground-state bleaching signal of the fused arrays larger than **T3** could not be measured beyond 1100 nm due to a lack of the detection sensitivity.

with the bands I. The transient absorption spectra of **T2** display three bleaching bands that correspond to their ground state absorption bands. For longer arrays, however, only two bleaching bands were detected due to a lack of sensitivity of a silicon diode array detector beyond 1200 nm. It is noteworthy that the featureless transient absorption in IR region becomes enhanced with an increase of the number of porphyrin moieties. To clarify the energy relaxation dynamics of each excited state of **T2**, the femtosecond time-resolved pump/probe experiments were also conducted by photoexcitation at 580 and 1100 nm which are in resonance with the bands II and III, respectively. Figure 5 displays the temporal profiles of the ground-state bleaching signals at 570 nm upon photoexcitations at 400, 580, and 1100 nm, respectively. All the temporal profiles are governed by a recovery process with $\tau = 4.5$ ps with a residual long-lived component regardless of the excitation wavelength.

Figure 6 shows the ultrafast anisotropy decays of **T2** monitored at 580 and 1100 nm by photoexcitation at 400 nm. As described in the above MO calculation, the transition dipole of the band I is aligned along the short axis (*y*-axis), whereas those of the bands II and III are parallel to the long molecular axis (*x*-axis). The abrupt anisotropy changes were actually observed with a time constant of ~0.2 ps reaching a plateau anisotropy value of −0.063 at 570 nm (band II) and with a time constant of ~0.5 ps reaching a plateau anisotropy value of 0.003 at 1100 nm (band III). The anisotropy value without rotation dynamics should be −0.2 if the orientation of the transition dipole moments of the bands I and II is perpendicular to each other.[25]

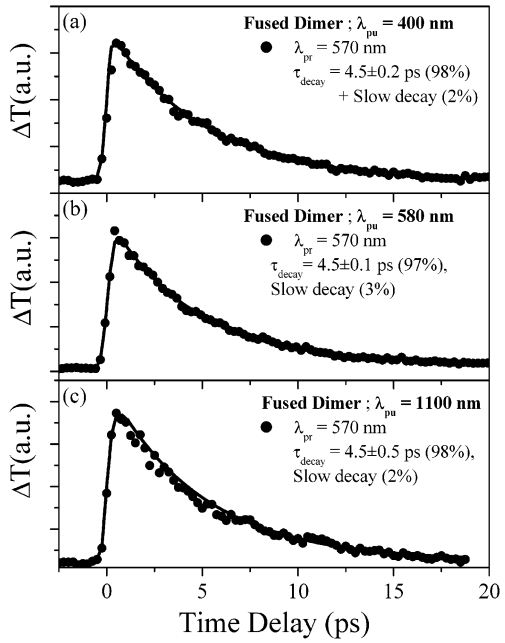

Figure 5. Ground-state bleaching recovery dynamics of **T2** at 570 nm are shown after photoexcitation at (a) 400 nm, (b) 580 nm, and (c) 1100 nm corresponding to the bands I, II, and III, respectively. The fast recovery dynamics with a lifetime of ~4.5 ps was observed regardless of the excitation wavelength, which indicates the ultrafast internal conversion processes to the ground state.

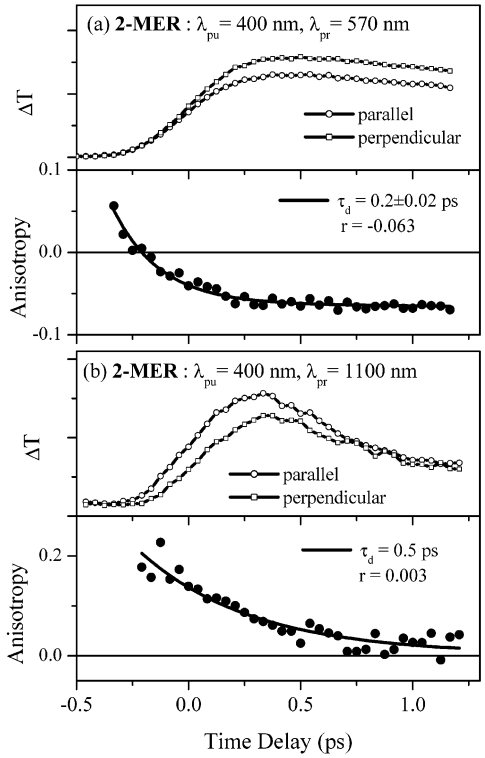

Figure 6. Transient anisotropy decay dynamics of **T2** after photoexcitation at 400 nm (the band I) were observed at (a) 570 nm (the II band) and (b) 1100 nm (the III band).

In the absorption spectra of the fused dimer, the broad intermediate states lie between the bands I and II. It is expected

(25) (a) Jonas, D. M.; Lang, M. J.; Nagasawa, Y.; Joo, T.; Fleming, G. R. *J. Phys. Chem.* **1996**, *100*, 12 660. (b) Min, C.-K.; Joo, T.; Yoon, M.-C.; Kim, C. M.; Hwang, Y. N.; Kim, D.; Aratani, N.; Yoshida, N.; Osuka, A. *J. Chem. Phys.* **2001**, *114*, 6750.

that the stimulated emission from the II state exists in this probe energy region as well as the ground-state bleaching. The stimulated emission of the II state gives rise to the initial fast anisotropy decay changing from positive to negative anisotropy value because of the transition from the I (or intermediate states) to II state, of which the transition dipoles are perpendicular to each other. The plateau anisotropy value at longer time delay is considered to be due mainly to the strong ground-state bleaching signal of the II and intermediate states. The theoretical calculation predicts that the orientation of the transition dipole moment of the intermediate states is parallel to the short molecular axis, like the I state. Thus, a deviation from an ideal plateau anisotropy value of −0.2 might be considered as the participation of the broad intermediate states residing between the I and II states in the energy relaxation process after photoexcitation at the band I.

Figure 6b shows the anisotropy decay at 1100 nm with a time constant of ∼0.5 ps at early times reaching a plateau anisotropy value of ∼0.003. At the 1100 nm probe wavelength, the transient absorption mainly comprises of the ground-state bleaching and the positive absorption from the III state to the II and broad intermediate states between the I and II states (ca. 8000−9000 cm^{-1}) as shown in Figures 1 and 3. The anisotropy value of ∼0.003 seems to be due to the sum of the bleaching (−0.2) and the photoinduced absorption contribution from the III state to the II and broad intermediate states of which the transition dipole orientation properties were not precisely determined. The initial anisotropy decay is dominated by the formation time of the III state, which can be considered as the internal conversion process from the I to III state. Thus, a difference in the time constants between the transient anisotropy changes at 570 and 1100 nm can be assumed to reflect the internal conversion process from the II to III state, although its difference is not so significant (∼0.2 ps vs ∼0.5 ps). Nevertheless, these observations indicate that the bottleneck process in the energy relaxation pathways upon photoexcitation at the band I is the internal conversion from the II to III state. It is also consistent with the experimental and calculated absorption spectra of the fused porphyrin arrays in that the density of states in UV/vis region is much larger than that in IR region.

Reflecting the well-separated absorption bands, **T2** exhibits the fluorescence from each state (the bands II and III) although the fluorescence quantum yields are very low ($\Phi_f \cong 10^{-5}$). The inset (a) of Figure 7 shows the fluorescence spectra from the II state in visible region. The femtosecond fluorescence up-conversion experiment was carried out to investigate the fluorescence dynamics. The inset (b) of Figure 7 displays the initial fluorescence decay process monitored at 650 nm upon photoexcitation at 400 nm, which exhibits roughly 300 fs initial decay along with a relatively long-lived component with a lifetime of 15 ps. The initial fast-decay component of ∼300 fs is consistent with the internal conversion process as observed in the anisotropy decay kinetics upon photoexcitation at ∼400 nm (Figure 6). On the other hand, a fast 200 fs rise component was not observed clearly, which is probably due to the limited time resolution of our fluorescence up-conversion setup. The overall fluorescence decay profile is displayed in Figure 7 in a longer time scale, which exhibits a major decay process with a time constant of 15 ps in addition to a minor long-lived component. The deactivation routes to exhibit the fluorescence

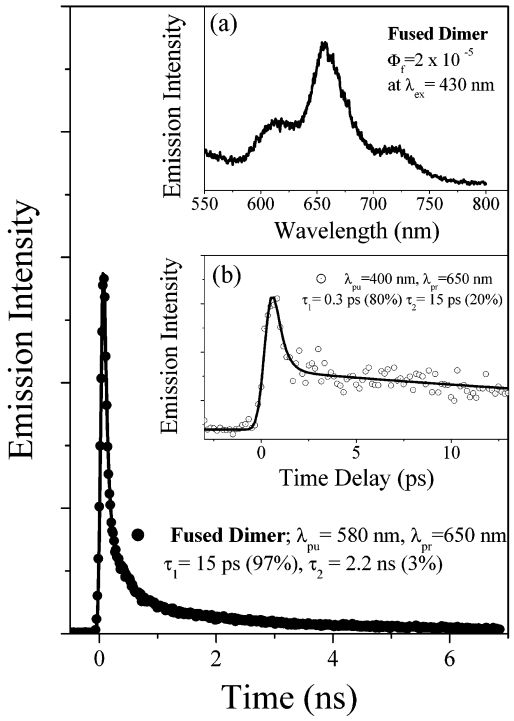

Figure 7. Fluorescence decay profile of **T2** with the main component of 15 ps in a long time window, which corresponds to the fluorescence from the band II. Inset 7(a) shows the fluorescence spectrum, in which the fluorescence quantum yield was estimated to be ∼2 × 10^{-5} by the comparison with that of free-base tetraphenylporphyrin. Inset (b) shows the fluorescence decay with the fast decay component of ∼0.3 ps from the II state measured by the fluorescence up-conversion method.

decay with a time constant of 15 ps have not been clearly elucidated yet. Because it has been well established that the vibrational cooling process in porphyrin molecules occurs in the time scale of 10−20 ps,[26] there is a possibility that the 15 ps component we observed is due to a partial contribution of the vibrational cooling process in the II state. As another candidate for this component, there is a possibility of impurity emission caused by photooxidation of **T2** in toluene solution, which, however, was not evinced by our experiment.

In any cases, we think that the involvement of many intermediate states below or near the state II in the decay of the state II provides complicated decay channels including the process via the state III. The long-lived component with a time constant of 2.2 ns is believed to be due to porphyrin monomers presumably arising from a minor photooxidation process. The dynamics of the IR fluorescence from the band III could not be measured due to a lack of sensitivity as well as a slow time response of a detector in IR region.

Excited-State Dynamics of Longer Fused Porphyrin Arrays. As continuing efforts to explore the excited-state dynamics of longer porphyrin tapes, we carried out the femtosecond UV/vis/IR pump/probe experiments for **T3**∼**T6**. Figure 8 shows a series of temporal profiles of the ground-state bleaching signals with a systematic change in the pump and probe wavelengths to be in resonance with the II states. In the transient absorption spectra of **T3** taken by photoexcitation at 695 nm,

(26) (a) Rodriguez, J.; Kirmaier, C.; Holten, D. *J. Am. Chem. Soc.* **1989**, *111*, 6500. (b) Rodriguez, J.; Kirmaier, C.; Holten, D. *J. Chem. Phys.* **1991**, *94*, 6020. (c) Eom, H. S.; Jeoung, S. C.; Kim, D.; Ha, J.-H.; Kim, Y.-R. *J. Phys. Chem. A* **1997**, *101*, 3661.

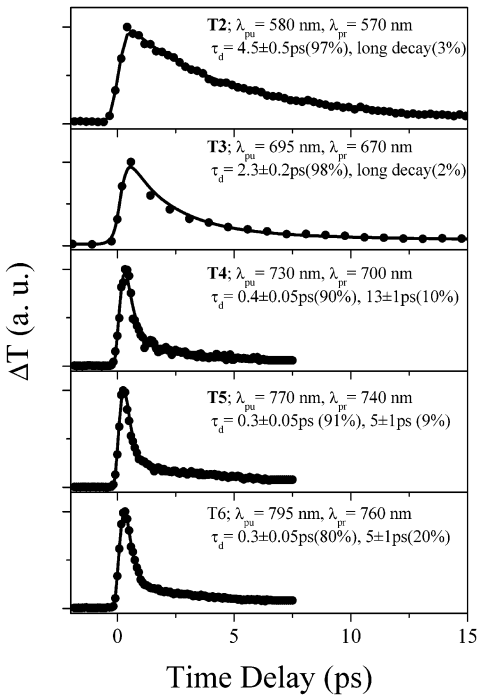

Figure 8. Ground-state bleaching recovery dynamics of **T2** (top) to **T6** (bottom) probed at the II bands after photoexcitation at the II bands. The ground state bleaching recovery time is gradually accelerated in going from **T2** to **T6**, showing a saturation effect in the arrays longer than **T4**. The time constants and pump/probe wavelengths are depicted in the inset.

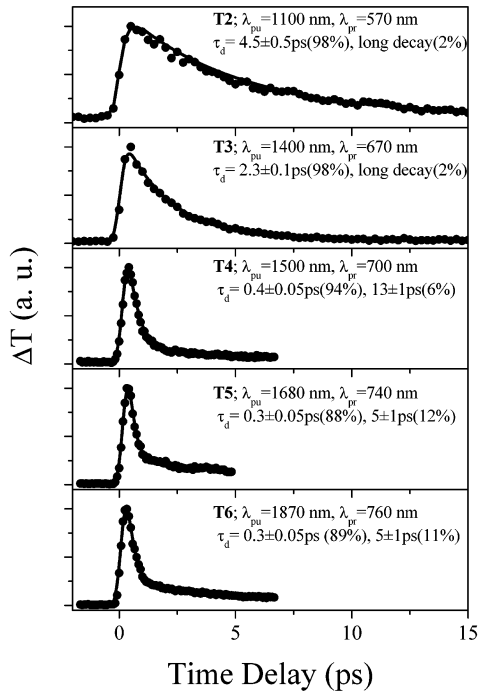

Figure 9. Ground-state bleaching recovery dynamics of **T2** (top) to **T6** (bottom) probed at the II bands after photoexcitation at the III bands. The ground state bleaching recovery time is gradually accelerated in going from **T2** to **T6**, showing a saturation effect in the arrays longer than **T4**. The energy relaxation dynamics by IR pump/visible probe are the same as those by visible pump/visible probe. The time constants and pump/probe wavelengths are depicted in the inset.

the temporal profiles of the bleaching signal monitored at 670 nm show a single-exponential recovery with a time constant of ~2.3 ps along with a negligible contribution by a long-lived component. The major recovery component of **T3** is ca. a half of that of **T2**. As the number of porphyrin units increases, the time constants of the major components are systematically reduced and become saturated with a value of ca. 0.3 ps in **T5** and **T6** (Figure 8). Similar measurements were performed by photoexcitation of the bands III. To tune the excitation wavelengths for the bands III, the pump wavelengths were changed continuously from 1.1 μm for **T2** to 1.87 μm for **T6** (Figure 9). The bleaching recovery processes at the bands II thus monitored are in a good agreement with those observed upon photoexcitation of the bands II. The femtosecond IR pump/IR probe experiments were also conducted. The temporal decay profile of **T3** probed at 1400 nm with photoexcitation at the same wavelength shows a decay profile similar to that monitored at 670 nm. However, the measurement of the recovery times of the IR bleaching signals of the porphyrin tapes longer than **T4** was severely perturbed by the enhanced photoinduced absorption signal in IR region. For even longer porphyrin tapes such as **T8** and **T12**, an oxidative decomposition of these arrays at room temperature is likely to preclude obtaining the reliable transient absorption data.

IV. Discussion

Electronic Transitions of Porphyrin Tapes. The systematic spectral changes of the Soret bands of the *meso*−*meso* linked porphyrin arrays have been explained in a qualitative manner by the simple point-dipole exciton coupling,[27] where the following eq 3 predicts the relationship of the splitting energy of the neighboring porphyrin units, ΔE_0

$$\Delta E_0 = \frac{\mu^2}{2\pi\epsilon_0 R^3} \tag{3}$$

where μ is the transition dipole moment and R is the center-to-center distance between the neighboring porphyins (8.35 Å). The splitting energy (ΔE) for longer arrays can be given by eq 4

$$\Delta E = \Delta E_0 \cos[\pi/(N+1)] \tag{4}$$

where N represents the number of porphyrin units. The observed Soret band splitting is actually lying on a linear line predicted by eq 4. This is arising from a situation that π-conjugation of the *meso*−*meso* linked porphyrin arrays is practically prohibited due to the perpendicular geometry between the adjacent porphyrins, which is a requisite for the exciton coupling, postulating that the spectral changes are induced only by the Coulombic interactions of the relevant transition dipole moments.

In contrast, the extensive π-conjugation is evident for the porphyrin tapes in view of the more red-shifted absorption spectra and the flat molecular shapes that ensure the coplanarity of the π-orbitals of the constituent porphyrin subunits. Despite this feature, the PPP−SCI calculation predicts the orientation of the transition dipole moments of the band I is aligned to the *y*-axis and that of the band II is aligned to the *x*-axis, which is similar to the situation of the unshifted and red-shifted Soret bands in the *meso*−*meso* linked porphyrin arrays. The observed linear plot of the energy difference between the bands I and II

(27) Kasha, M.; Rawls, H. R.; El-Bayoumi, M. A. *Pure Appl. Chem.* **1965**, *11*, 371.

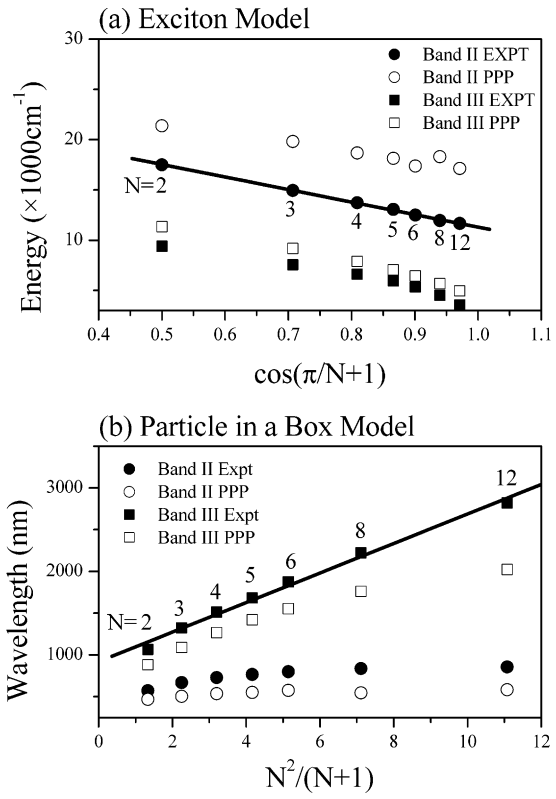

Figure 10. Plots of the energies of the absorption bands II and III of the porphyrin tapes as a function of the number of porphyrin units show a good correlation between the experimental data and PPP−SCI calculated values. The electronic character of the band II is explained by the splitting energy of the exciton model (a) while that of the band III is well fitted by a particle in a box model (b).

as a function of the exciton splitting energy based on eq 4 indicated that the absorption spectral shapes are actually influenced by the number of porphyrin units and the constituent porphyrin pigments are aligned in a regular arrangement in the series (Figure 10a). On the contrary, the plot of the bands III deviates strongly from the exciton coupling scheme. Instead, the plot based on the free electron model (a particle in a box model) gives rise to a well-correlated straight line, indicating that the excited state corresponding to the band III can be characterized by the extensive π-conjugation throughout the entire porphyrin tapes (Figure 10b). Thus, the lowest excited state of the directly *meso*−*meso* linked porphyrin arrays can be considered as a Frenkel-type exciton, in which the exciton binding energy is relatively large (∼1 eV) with a small exciton Bohr radius, whereas the lowest excited state of **Tn** is a close resemblance of a Wannier-type exciton with a very low exciton binding energy (∼0.1 eV or less) and a large exciton Bohr radius. Thus, much broad electronic transitions observed in **Tn** are characteristic of Wannier-type excitons with a large variation in the exciton Bohr radius.

As shown in Figure 10a, the PPP−SCI calculated energy shift of the band II is qualitatively in agreement with that of experiment. The $\boldsymbol{P}_{e-h}$ plots for the excited states of **S8** and **T8** are shown in Figure 11, showing how much each state has the CT character. As expected, all three bands of **S8** exhibit largely the LE nature (Figure 11a). The essentially LE nature of the II state of **T8** with less significant contribution of long-range CT is clearly evidenced by the $\boldsymbol{P}_{e-h}$ plot (Figure 11b). It is worthwhile to point out that the II states in **T6** show essentially the same $\boldsymbol{P}_{e-h}$ plot as that shown in Figure 11b, and it is also the case of **T4** where the component state with smaller oscillator strength exhibits more enhanced CT character. Then, it may be considered that significant configuration interaction between LE and CT configurations gives rise to many excited states around the band II position. Because such a feature would be overestimated by the present computational method as seen from the **T6** spectrum, the intersubunit CT contribution to the II state depicted in Figure 11 would be also overestimated.

Although the band I is dominated by a single excited state up to **T4**, we find that its CT character is progressively enhanced upon an increase in the number of porphyrin subunits from the $\boldsymbol{P}_{e-h}$ plot for these excited states. For **T6**, **T8**, and **T12**, the band I clearly exhibits resonant feature in consistent with the enhancement of CT contribution (Figure 3). The $\boldsymbol{P}_{e-h}$ plot for one of the I states of **T8** (indicated by an arrow in Figure 3), which exhibits intermediate CT character among the main twelve component states, is shown in Figure 11b. On the basis of averaging over the component states, we can say that the CT character of the I band is more significant than that of the II band.

As seen from the $\boldsymbol{P}_{e-h}$ plot in Figure 11b, the III states of **Tn** can be characterized by a charge-transfer exciton being qualitatively similar to the case of the lowest dipole-allowed singlet excited state of π-conjugated polymers such as poly(*p*-phenylene vinylene) (PPV).[22] As shown in Figure 10b, the PPP−SCI calculated III band wavelength scales linearly up to **T6** in agreement with the experimental value, while its deviation from the experimental value starts to increase beyond **T8** showing much faster saturation. This indicates that an effective Coulomb interaction in longer fused porphyrin arrays should be gradually attenuated upon an increase in the number of porphyrin subunits leading to a Wannier-exciton like character of the III state for sufficiently long arrays.

Thus, the porphyrin tapes do not show any indication of effective conjugation length (ECL) effect, suggesting further lowering of the band gap energy in even longer arrays. Because the electronic transitions of longer fused arrays reach into the vibrational energy levels corresponding to CH vibration at ∼3000 cm^{-1}, this unique electronic transition is expected to give a clue to the vibronic coupling of large molecules.

Internal Conversion Processes of Fused Porphyrin Arrays. There is a relatively large energy separation in metalloporphyrins between the S_2 (B-band) and S_1 (Q-band) excited states in UV−vis region. In addition, these two states are considered as a 50−50 admixture of two common excited electronic configurations $^1(a_{1u},e_g)$ and $^1(a_{2u},e_g)$ in accidental degeneracy and the energy surfaces of the S_1 and S_2 excited states are almost parallel especially in *meso*-aryl-substituted porphyrin monomers. This definitely retards the $S_2 \rightarrow S_1$ intramolecular electronic internal conversion processes. The S_1 state of Zn(II)*meso*-tetraphenylporphyrin monomer is formed with a time constant of ∼1.6 ps following the Soret (S_2) band excitation and decay to the ground state on a much slower time scale of 2.64 ns.[13]

In the directly linked porphyrin arrays **Sn**, the internal conversion rates were reported in our early paper by femtosecond fluorescence up-conversion method.[12(b)] The internal conversion rates of **Sn** are larger than that of porphyrin monomer, which could be explained by the concept of a "ladder" acting

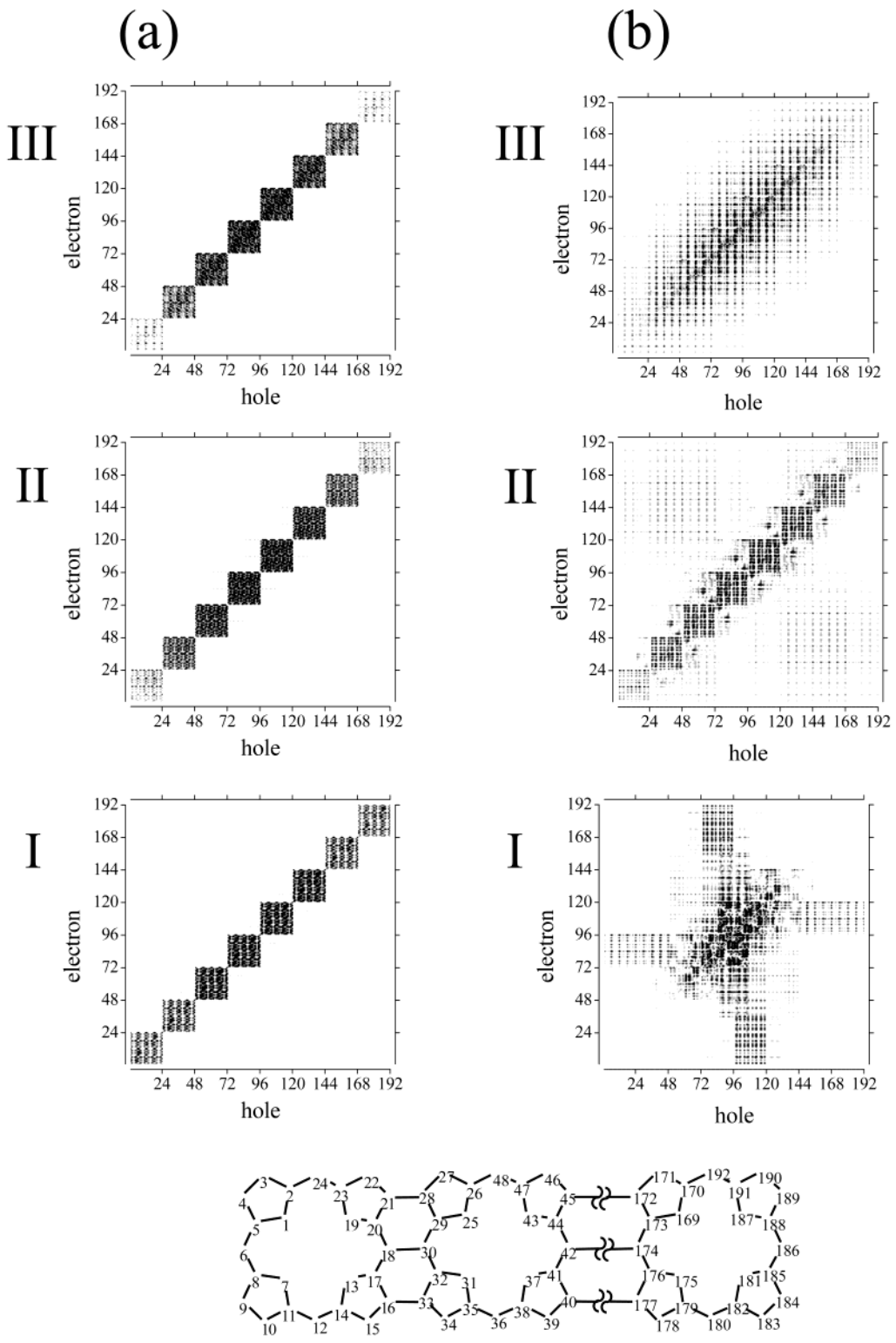

Figure 11. PPP−SCI calculated charge-transfer probability $\boldsymbol{P}_{e-h}$ (r, s), which is defined by eqs 1 and 2, for the excited states contributing to the I, II, and III bands for **S8** (a) and **T8** (b). The shading at each grid (r, s) represents the probability of simultaneously finding an electron at r-th atomic site and a hole at s-th site. The numbering of atomic sites for **T8** is also indicated and the numbering way for **S8** is the same as that for **T8**.

as the intermediate states. The splitting of the component levels of the Soret manifold establishes a band of intermediate levels between the monomeric Soret band (B_y) and the exciton-split Soret band (B_x) in **Sn**. In addition, our INDO/S−SCI calculation[24] has revealed that CT bands (inter-porphyrin moiety one-electron transition) are accidentally located in the same energy region as a result of a close proximity of the neighboring porphyrin subunits in **Sn**. These Soret and CT states provide a "ladder" for sequential relaxations between successive pairs of levels that are separated by energies much smaller than the S_2-S_1 gap of conventional porphyrin monomer.

The internal conversion process of **T2** was observed indirectly by the time-resolved anisotropy decay measurement technique (Figure 6) and the fluorescence up-conversion technique (Figure

7). As described above, the present PPP calculations predict that the overlapping of CT and Soret bands is also the case of **T2** which has essentially the same inter-porphyrin distance as that of **S2**. Then, the "ladder" type acceleration of I → II internal conversion process should be sufficiently enhanced also in **T2**. As the arrays become longer, the number of Soret and CT states increases in proportion to the number of porphyrin subunits as shown in Figure 3. Because the CT bands are essentially located in the high-energy side of the II band, the density of states is much higher in the energy region between the I and II bands than that between the II and III bands (Figure 3 and Table 1). These computational results are consistent with the experimental observations (Figure 1) which show more significantly enhanced absorption in the interval wavelength region between the I and II bands than that between the II and III bands. Therefore, on the basis of the experimental results for **T2** and the PPP−SCI calculations, the rate determining step in the overall internal conversion processes upon photoexcitation of the I states in **Tn** is likely to be the II → III internal conversion process as in the case of **T2**. However, it becomes more difficult to determine the bottleneck internal conversion process as the arrays become larger, because the energy gap between the II and III states becomes reduced and the number of intermediate states between the two states increases as observed in the absorption spectra.

Extremely Rapid Decay of the Lowest Excited States. The energy relaxation dynamics of the lowest excited states of the porphyrin tapes are accelerated as the number of attached porphyrin units increases, which is consistent with the energy gap law (Figures 8 and 9). For instance, the lowest excited electronic state of **T2** decays to the ground state with a time constant of 4.5 ps, which is much faster than that of the orthogonal dimer (1.9 ns). Upon elongation of the porphyrin tapes, the decay times of the lowest excited electronic states decrease significantly, viz., 2.3 ps for **T3**, 0.4 ps for **T4**, and 0.3 ps for **T5**, and 0.3 ps for **T6**. The lifetimes of the lowest excited electronic states of **1** and **S2**∼**S6** are in a range of 2.64∼1.66 ns.[12(b)] On the contrary, the lifetimes of the lowest excited states of **Tn** are much shorter and reach ca. ∼0.3 ps for **T5** and **T6** (Figures 8 and 9). Thus, the contribution by the vibration cooling of **Tn** in the S_0 state to the internal conversion process, if any, of the porphyrin tapes should be minimal. These results indicate that the decay rates of the S_1 states of the porphyrin tapes are enhanced as the S_1 state energy is lowered.

Until now, the ultrafast internal conversion process with a time constant of picosecond was observed in the cases of azulene[28−30] and DNA bases[31,32] which have large S_1-S_0 energy gaps of ∼15 000 and ∼34 000 cm^{-1}, respectively. The probable mechanisms to explain the unusually short lifetimes were proposed such as the conical intersection between the S_0 and S_1 states,[28,29] the vibronic coupling between $\pi\sigma^*$ and $\pi\pi^*$ states[33] and the energy gap law formalism of radiationless transition theory.[30] In the fused porphyrin arrays, it is possible to explain the ultrafast internal conversion in terms of the energy gap law which means that there is a strong correlation between the ordering of the S_1 state energies and that of their lifetimes.

(28) Beer, M.; Longuett-Higgins, H. C. *J. Chem. Phys.* **1955**, *23*, 1390.
(29) Bearpark, M. J.; Bernardi, F.; Clifford, S.; Olivucci, M.; Robb, M. A.; Smith, B. R.; Vreven, T. *J. Am. Chem. Soc.* **1996**, *118*, 169.
(30) Tittelbach-Helmrich, D.; Steer, R. P. *Chem. Phys.* **1995**, *197*, 99.
(31) Pecourt, J.-M. L.; Peon, J.; Kohler, B. *J. Am. Chem. Soc.* **2000**, *122*, 9348.
(32) Peon, J.; Zewail, A. H. *Chem. Phys. Lett.* **2001**, *348*, 255.
(33) Sobolewski, A. L.; Domcke, W. *Chem. Phys.* **2000**, *259*, 181.

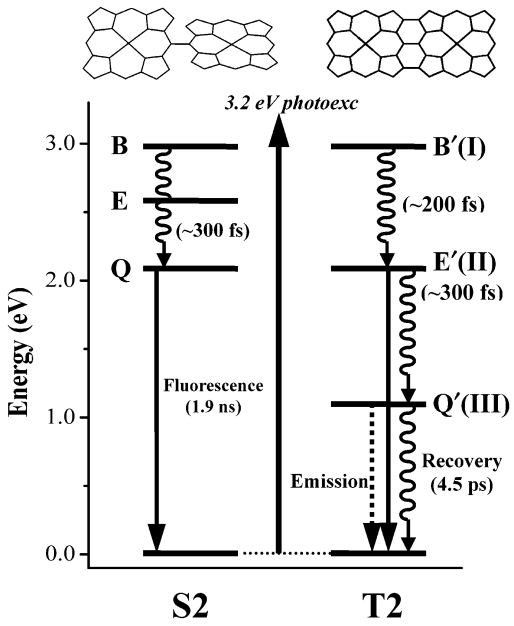

Figure 12. Energy relaxation dynamics of *meso*−*meso* directly linked porphyrin dimer (**S2**) and triply linked fused porphyrin dimer (**T2**). In **S2** the internal conversion process occurs very fast with a time constant of ∼300 fs and decays slowly with a time constant of ∼1.9 ns from the Q state to the ground state. In **T2**, however, the internal conversion time constant from B′(the I state) to Q′(the III state) was estimated to be ∼500 fs in the transient anisotropy decay dynamics and then the internal conversion process occurs with a time constant of ∼4.5 ps to the ground state, which is the major difference in the excited-state dynamics between the two porphyrin dimers.

The absorption spectra of the fused porphyrin arrays show that the absorption tail of the band III becomes gradually wider, indicating the increased density of states near the lowest excited states of the fused porphyrin arrays. In addition, the 0−0 absorption band downshifts from 9400 cm^{-1} for **T2** to 5300 cm^{-1} for **T6**. Thus, the combination of the reduced energy gap and the increased density of states near the lowest excited states is likely to facilitate the electronic deactivation processes from the lowest excited state to the ground state as the fused porphyrin arrays become longer. At the same time, because the energy difference between the lowest excited and ground states becomes significantly reduced in the fused porphyrin arrays, the electronic vibronic coupling process becomes enhanced. This process provides more effective nonradiative deactivation channels for larger molecules because they have rich vibrational motions that can couple to the electronic states as the electronic energy levels become lowered. A schematic diagram for the overall energy relaxation dynamics of **Sn** and **Tn** is displayed in Figure 12 as representative examples of **S2** and **T2**.

V. Conclusions

Various photophysical properties of the fused porphyrin arrays up to **T6** were investigated by using time-resolved spectroscopic measurements. The overall relaxation dynamics of the porphyrin tapes show a systematic change as the number of porphyrin pigments increases in the arrays. The internal conversion processes from the initially populated highly excited I states of the arrays to the lowest excited III states were observed to be very fast compared with those of monomer due to the participation of the increased density of states as a "ladder" type deactivation channel. The energy relaxation dynamics of the

lowest excited states of the porphyrin tapes were mainly determined by the energy difference from their ground states. The overall photophysical properties of the porphyrin tapes are in contrast with those of the orthogonal porphyrin arrays. Although the orthogonal porphyrin arrays have proven to be promising as a candidate for efficient molecular photonic wires due to their strong excitonic interactions between the adjacent porphyrin moieties, the porphyrin tapes provide a good prospect for molecular electric wires due to much reduced band gap energy between HOMO and LUMO levels. Because the lowest electronic transitions in the porphyrin tapes occur closer to the vibrational excitations, these molecules can be good candidates for the investigation of vibronic coupling in large organic molecules. The active participation of the high density of CT states in the energy relaxation dynamics of photoexcited porphyrin tapes is expected to give rise to large optical nonlinearity along with a fast response time. As already observed in *p*-nitroaniline, the donor−acceptor type CT state also exhibits fast deactivation process of photoexcited *p*-nitroaniline which has already proven to be promising molecule for large optical nonlinearity.[34] The investigation of the third order nonlinear optical properties of the orthogonal and fused porphyrin arrays by Z-scan method are currently under way at our laboratory. Overall, the unique photophysical properties of the porphyrin tapes deserve much attention for the future applications as IR sensors and nonlinear optical materials.

Acknowledgment. The work at Yonsei University has been financially supported by the National Creative Research Initiatives Program of the Ministry of Science & Technology of Korea. The work at Kyoto was supported by the CREST (Core Research for Evolutional Science and Technology) of Japan Science and Technology Corporation (JST). K.T. acknowledges the support by a Grant-in-Aid for Scientific Research (B) from Japan Society for the Promotion of Science (JSPS).

JA020826W

(34) (a) *Nonlinear Optical Effects of Organic Materials and Crystals*; Chemla, D. S., Zyss, J., Eds.; Academic Press: Orlando, FL, 1994; Vols. 1 and 2. (b) Kovalenko, S. A.; Schanz, R.; Farztdinov, V. M.; Hennig, H.; Ernsting, N. P. *Chem. Phys. Lett.* **2000**, *323*, 312. (c) Thomsen, C. L.; Thøgersen, J.; Keiding, S. R. *J. Phys. Chem. A* **1998**, *102*, 1062.